A Novel Damping Device for Broadband Attenuation of Low-Frequency Combustion Pulsations in Gas Turbines

Mirko R. Bothien, Nicolas Noiray, Bruno Schuermans

Alstom, Baden, Switzerland

Abstract

Damping of thermoacoustically induced pressure pulsations in combustion chambers is a major focus of gas turbine operation. Conventional Helmholtz resonators are an excellent means to attenuate thermoacoustic instabilities in gas turbines. Usually, however, the damping optimum is in a narrow frequency band at one operating condition. The work presented here deals with a modification of the basic Helmholtz resonator design overcoming this drawback. It consists of a damper body housing separated volumes that are connected to each other. Adequate adjustment of the governing parameters results in a broadband damping characteristic for low frequencies. In this way, changes in operating conditions and engine-to-engine variations involving shifts in the combustion pulsation frequency can conveniently be addressed. Genetic algorithms and optimization strategies are used to derive these parameters in a multi-dimensional parameter space. The novel damper concept is described in more detail and compared with cold-flow experiments. In order to validate the performance under realistic conditions, the new broadband dampers were implemented in a full-scale test engine. Pulsation amplitudes could be reduced by more than 80%. In addition, it is shown that due to sophisticated damper placement in the engine two unstable modes can be addressed simultaneously. Application of the damper concept allowed to considerably increase the engine operating regime and finally to reduce NO_x emissions by 55%. Predictions obtained with the physics-based model excellently agree with experimental results for all tested damper geometries, bias flows, excitation amplitudes, and most important with the measurements in the engine.

1. Introduction

One of the major challenges in the development process of modern gas turbines is the stability of the combustion process. In order to achieve best-in-class NO_x emissions, the engine is operated lean-premixed. In this operation mode, the combustion process is susceptible to self-induced oscillations arising due to the interaction of unsteady heat release and acoustic field in the combustion chamber. If the two mechanisms constructively interfere, high amplitude pressure and heat release fluctuations might occur, which have a detrimental effect on the combustion process. These so-

This is a pre-print version. Published in *Journal of Engineering for Gas Turbine and Power* (2014) Vol. 136 (4) Article number 041504, DOI: 10.1115/1.4025761

called thermoacoustic instabilities restrict the engine operating regime and can in the worst case cause structural wear.

In principle, there are two ways of counteracting, namely, active and passive control methods that aim to disrupt the thermoacoustic feedback cycle, e.g., by dissipation of acoustic energy. Due to requirements with respect to robustness, reliability, and costs, usually, passive methods are applied in gas turbines [1, 2]. Typical passive damping devices are Helmholtz resonators; the most basic form being a volume that is connected to an enclosure via a so-called neck. By doing so, a frequency dependent acoustic boundary condition is imposed that can be adjusted such that it features low reflection, i.e., high absorption, of acoustic energy. A very descriptive way to understand the underlying principle is the analogy with a spring-mass (volume-neck) system featuring a damping term. At the neck, where the acoustic velocity is highest, the major part of acoustic energy dissipation occurs. The mass oscillating inside the neck causes acoustic energy to be transformed into vortices shedding from the neck's edges that are finally dissipated into heat [3, 4, 5, 6]. Basic derivations for the damper's resonance frequency and absorption behaviour can, for instance, be found in Refs. [7, 1, 8].

An abundant amount of literature on theoretical and modeling aspects of Helmholtz resonators as well as lab-scale experiments exists. However, publications on application to full-scale land-based gas turbines and their performance are scarce; Bellucci et al. and Bothien et al. [1, 2, 9] being the only ones who (at least lately) reported on successful engine results. This lack was also mentioned in an extensive review on passive control methods by Richards et al. [10]. In contrast to this, application to sector or atmospheric annular rigs can be found [11, 12, 13]. In Ref. [13], it is explicitly stated that although having been successfully tested in annular engine-scale test rigs, prior to using Helmholtz resonators inside the engine some open challenges have to be addressed. Pandalai & Mongia [14] show that multiple "damper tubes" (i.e., quarter wave resonators) are installed in their aero-derivative engines to abate thermoacoustic pulsations.

Although common Helmholtz resonators are an excellent means to attenuate thermoacoustic pulsations, they are only effective in a narrow frequency band. The lower the frequency of interest, the smaller is the resonator's frequency bandwidth. Pulsation frequencies observed in gas turbines typically are below 500 Hz for which this damping range is of the order of a few Hertz. Engine-to-engine variations that are, for instance, caused by different ambient conditions or different fuels, might involve shifts in the combustion pulsation frequency. Thus, adaptations of the damper hardware might be required for each single case. Consequently, a narrowband damper usually has its optimum damping characteristic only at one operating condition.

This work deals with a modification of the basic Helmholtz resonator design for broadband low-frequency ranges. It consists of a damper body housing multiple separated volumes. The single volumes are connected to each other by means of secondary necks. By adequately adjusting the governing parameters, i.e., neck geometries, bias flows, and volume ratios, using a multi-parameter optimization routine the coupling between the single volumes is influenced so that a broadband damping character for low frequencies is obtained. Because of this, the resulting frequency range of

This is a pre-print version. Published in *Journal of Engineering for Gas Turbine and Power* (2014) Vol. 136 (4) Article number 041504, DOI: 10.1115/1.4025761

effective damping of one damper can be increased to 50-150 Hz. Hence, above mentioned drawbacks are overcome. In addition to this, simulations of an engine equipped with a number of dampers show that the damping efficiency of the presented multi-volume configuration can be considerably higher than that of single-volume dampers with equal dimensions.

The concept of coupled Helmholtz resonators has been studied by other authors as well [11, 15, 16]. In the works cited, two volumes are connected to each other. However, application to full-scale gas turbines or combustion systems in general has not been reported before. In aero-engines, extensive use of acoustic liners is made to attenuate the flow induced noise emitted from the nacelle. Although not widely applied in the engine due to various reasons, work has been done on so-called two- or multi-degree-of-freedom liners [17, 18] which in essence are serial damper configurations.

The work and results reported here emphasize Alstom's long term strategy with respect to an in-depth understanding of engine thermoacoustics and suitable countermeasures against combustion pulsations. In Refs. [19, 20], a method to assess the damping performance of generic Helmholtz dampers coupled to an engine was introduced. This method is further developed and incorporates an accurate model mimicking the acoustic characteristics of a multi-volume damper. Recently, we published articles on optimum damper placement in annular combustion chambers [21, 22] outlining the importance of damper locations on their performance. The principles explained therein are also used in this work. Finally, the prediction of the onset of a second mode caused by the suppression of the dominant one [23] and its importance for full-scale gas turbines could be experimentally verified.

2. Acoustic damper model

It is common practice to represent the (thermo-)acoustic behaviour of combustion systems by making use of network models (see Ref. [24] for an literature overview of different approaches in the combustion community). At Alstom, the in-house code $Ta3$ was developed for this purpose and is, in this paper, used to simulate the acoustic characteristics of the damper. This Matlab/Simulink based tool describes a system's (thermo-)acoustics as a modular network of subsystems into which the system is divided. Usually, $Ta3$ is used to mimic the thermoacoustics of full-scale engines. It consists of a hybrid approach: numerical, experimental and analytical techniques are combined to describe the real system. A brief general description of $Ta3$ is given in the following paragraph. For an in-depth treatment and explanation of the code, the interested reader is referred to Refs. [2, 23]. Therein, also comparisons of $Ta3$ simulations with engine data are shown demonstrating the tool's capabilities to efficiently reproduce thermoacoustic coupling in gas turbines.

The acoustic variables for the single network modules, i.e., acoustic pressure p and particle velocity u, are expanded on a modal basis to obtain a state-space representation of the acoustic propagation. By doing so the acoustic input-output behaviour of a subsystem is described. If the geometry of a respective subsystem is sufficiently simple, its acoustics can be described analytically.

This is a pre-print version. Published in *Journal of Engineering for Gas Turbine and Power* (2014) Vol. 136 (4) Article number 041504, DOI: 10.1115/1.4025761

For complex three-dimensional geometries, finite element calculations (FEM) are used. In this case, the FEM results are converted into state-space models which can be connected to other network blocks. The acoustic characteristics of the flame are incorporated by means of flame transfer functions and source terms which are obtained by fitting state-space models to measured data. Depending on the size of the modal expansion, the state order of the multiple input multiple output subsystems is defined. The different modules used to model the thermoacoustic system relate upstream and downstream acoustic velocities and pressures. They are connected to each other by using the Redheffer star product. The state-space network approach allows either for time domain simulations including non-linearities or frequency domain calculations. For the latter, an eigenvalue analysis to assess the system stability can be performed, which is straightforward due to the state-space formulation.

Figure 1 shows a schematic build-up of the damper model for the acoustic wave propagation inside the damper. It consists of an upstream boundary condition, N subsystems S_i, and the interconnection to the combustion chamber (CC). Note that only analytical blocks are used. The

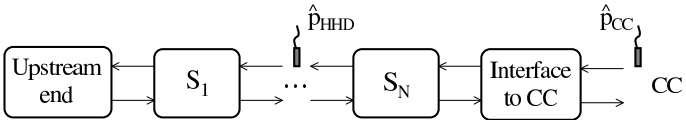

Figure 1: Schematic block diagram for the damper model.

arrows connecting the single subsystem represent the primitive acoustic variables, i.e., acoustic pressure and particle velocity. The number of subsystems depends on the complexity of the inner damper geometry. For model validation and assessment of the damper performance, the acoustic pressures inside the damper p_{HHD} and combustion chamber p_{CC} are recorded.

A key aspect of this modelling approach is that the wave propagation through a volume of any complexity is represented as a multi-input multi-output system between N velocity inputs and N pressure outputs. Such a system can conveniently be expressed in state-space form as:

$$\begin{aligned} \frac{\partial}{\partial t}\begin{bmatrix} \vec{\eta} \\ \dot{\vec{\eta}} \end{bmatrix} &= \begin{bmatrix} \mathbf{0} & \mathbf{I} \\ -\mathbf{\Omega} & \mathbf{0} \end{bmatrix}\begin{bmatrix} \vec{\eta} \\ \dot{\vec{\eta}} \end{bmatrix} + \begin{bmatrix} \mathbf{0} \\ \mathbf{\Psi}^T\,\mathbf{A} \end{bmatrix}\vec{u} \\ \frac{\vec{p}}{\rho\, c} &= c\,[\mathbf{0}, \mathbf{\Psi}]\begin{bmatrix} \vec{\eta} \\ \dot{\vec{\eta}} \end{bmatrix}, \end{aligned} \tag{1}$$

where $\mathbf{\Psi}$ is a $N \times K$ matrix whose K columns contain $\frac{\psi_k(\mathbf{x_n})}{\Lambda_k}$, and $\psi_k(\mathbf{x_n})$ is the value of the k^{th} mode at location $\mathbf{x_n}$ on the boundary and $\Lambda_k^2 = \int \psi_k^2(\mathbf{x}) d\,\mathbf{x}$ is a normalization factor for the modes. The diagonal matrix $\mathbf{A}$ contains the area corresponding to the n velocity inputs. The $K \times K$ diagonal matrix $\mathbf{\Omega}$ contains the eigenfrequencies of the solid–walled geometry, $\mathbf{I}$ and $\mathbf{0}$ are the $K \times K$ unit matrix and zero matrix, respectively. The vectors $\vec{\eta}$, $\vec{p}$ and $\vec{u}$, contain the modal amplitudes, the input velocities u_m and the output pressures p_n. The quantities ρ and c are the

This is a pre-print version. Published in *Journal of Engineering for Gas Turbine and Power* (2014) Vol. 136 (4) Article number 041504, DOI: 10.1115/1.4025761

medium's density and speed of sound, respectively. In the limit case of K approaching infinity, the system of equations (1) is an exact solution of the wave equation with negligible Mach number. The solution converges rapidly, so in practice only a limited number of modes K is required in the modal expansion.

The Mach number in gas turbine combustion applications is typically sufficiently low to ensure a negligible effect on acoustic wave propagation. However, Mach number effects cannot be neglected on inlet/exit conditions and at area discontinuities. The losses at area discontinuities are especially important when modelling dampers. In the time domain (denoted by the $(\cdot)'$), the relation between the acoustic velocities on both sides of the discontinuity (denoted by u'_1 and u'_2) and the acoustic pressures (denoted by p'_1 and p'_2) can be modelled by casting the unsteady Bernoulli equation in the following non-linear state-space equation:

$$\begin{aligned} \frac{\partial u'_1}{\partial t} &= \frac{-\frac{1}{2}\,\bar{\rho}\,\zeta((\bar{u}+u')|\bar{u}+u'|-\bar{u}|\bar{u}|)+p'_1-p'_2}{L_v\,\bar{\rho}} \\ u'_2 &= \frac{A_2}{A_1}\,u'_1, \end{aligned} \tag{2}$$

in which ζ is a loss coefficient (typically obtained from correlations found in literature, or from experiment), L_v is the virtual acoustic length, which takes into account the inertia of the mass of air fluctuating at the discontinuity (it can be obtained from correlations, experiment or from acoustic FEM calculations).

The more subsystems the model exhibits the higher is its order and the longer is the calculation time. This becomes important when a multi-parameter optimization routine should be used to find the optimum damper parameters to damp at certain frequencies or in a broad frequency range. A trade-off between accuracy and model order is necessary. Therefore, once the model of the damper is obtained, adequate model reduction techniques as, e.g., balanced truncation [25], are used in order to reduce the number of states.

3. Comparison of model and experiments

The acoustic properties of various damper variants are measured in a cold-flow acoustic test facility. The prime objective of these isothermal experiments is to obtain a physics-based damper model that covers a sufficiently wide range of combinations of the governing parameters influencing the damper's performance. Therefore, the test damper is build up modularly allowing to individually change all important parameters. This includes different geometries and numbers of the first and secondary necks, volume ratios, and bias flow velocities.

Figure 2 shows a schematic of the measurement setup. In the test rig, woofers provide the acoustic excitation in the required frequency and amplitude spectrum. The acoustic field inside the rig is measured by 1/4" Brüel & Kjær condenser microphones located on several axial positions. By means of the multi-microphone method (MMM) [26] the acoustic field is decomposed into the

This is a pre-print version. Published in *Journal of Engineering for Gas Turbine and Power* (2014) Vol. 136 (4) Article number 041504, DOI: 10.1115/1.4025761

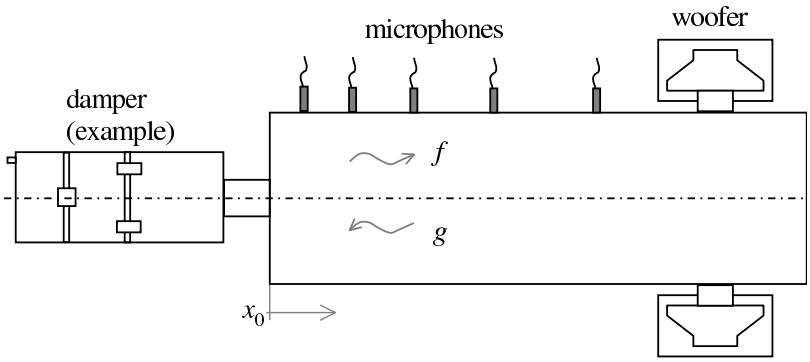

Figure 2: Schematic of measurement setup in cold-flow acoustic test facility.

up- and downstream travelling waves, g and f The Riemann invariants f and g are related to the primitive acoustic variables – pressure p and particle velocity u – by $p/\rho c = f + g$ and $u = f - g$. This allows to calculate the reflection coefficient R at the reference location x_0 in the frequency domain:

$$R = \frac{g}{f}. \tag{3}$$

By using the MMM to determine the Riemann invariants f and g an overdetermined system of equations is solved in a least-squares sense. The error between measured and reconstructed acoustic pressure can be calculated as is, e.g., done in [24]. Besides noise contributions, possible relevant error sources are the determination of the speed of sound and the microphone calibration coefficients. The resulting relative error for the results shown here is approximately 2%.

A suitable control routine is applied to prescribe a constant, frequency-independent pressure amplitude in front of the damper. The latter enables to accurately study nonlinear effects, which might be important if the fluctuation inside the damper neck is not small compared to the main neck velocity.

In most of the cases, the space available to install dampers inside the engine is limited. Thus, the development objective is to realize the optimum performance, both in frequency range and damping within the given limitations.

Model accuracy under isothermal conditions

In Fig. 3, the measured reflection coefficients (dashed with ×) are compared to model predictions (solid) for three different damper configurations. For all curves, the order of the model's state-space system is 6. The difference between the subfigures (a)-(c) is the geometry of the main and secondary necks including neck diameters, lengths, and edge shapes; the overall damping volume remains constant. The different colours in each of the subfigures represent different ratios of the volumes out of which the damper is composed. It can be seen that the low-order model excellently corresponds to the measured reflection coefficients; both in magnitude and phase. The

This is a pre-print version. Published in *Journal of Engineering for Gas Turbine and Power* (2014) Vol. 136 (4) Article number 041504, DOI: 10.1115/1.4025761

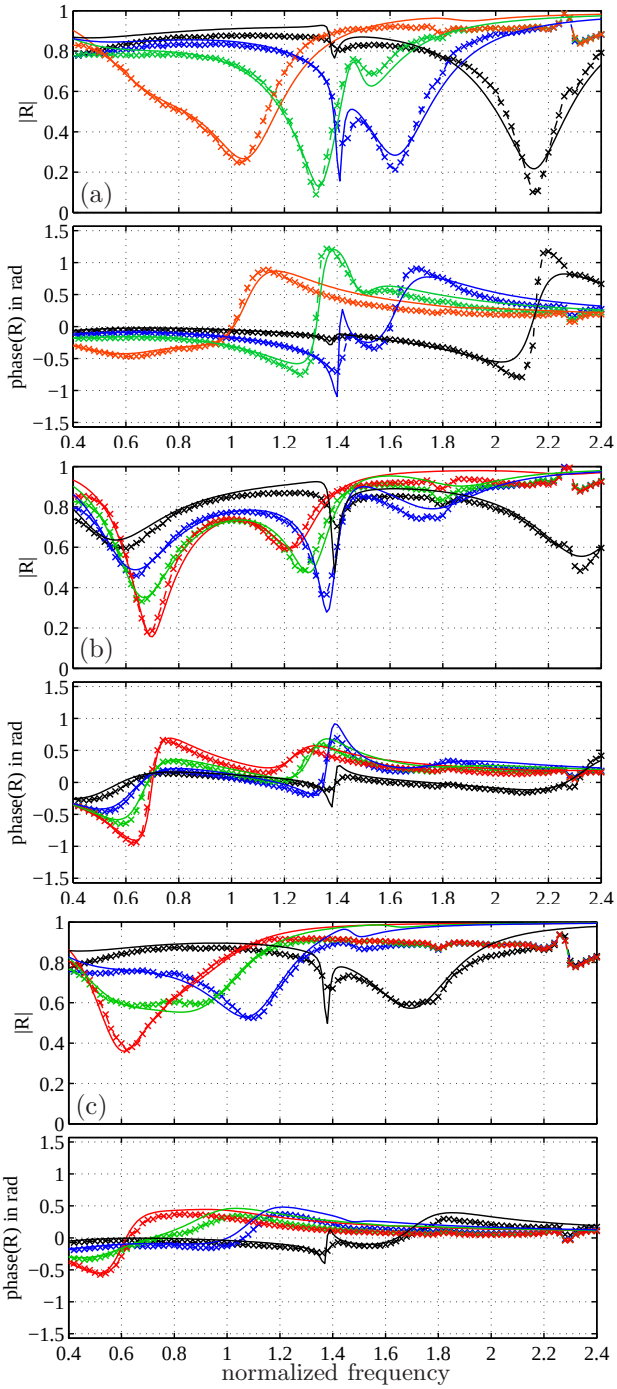

Figure 3: Comparison of measured reflection coefficients (dashed with ×) and model (solid) for different geometries (a)-(c); top: magnitude, bottom: phase. From red to blue, the ratio between most downstream to most upstream volume decreases.

This is a pre-print version. Published in *Journal of Engineering for Gas Turbine and Power* (2014) Vol. 136 (4) Article number 041504, DOI: 10.1115/1.4025761

characteristic dent observed at a normalized frequency of around 1.4 is caused by the fact that the length dimension of the damper corresponds to the quarter wave-length at this frequency.

Generally, the acoustic response of dampers is strongly affected by the pressure loss coefficients and the effective lengths of the necks. In a single-volume setup, the former mainly determines the damping performance whereas the latter has a governing influence on the damper's resonance frequency. In a multi-volume damper, both also strongly influence the coupling between the single volumes. Although an abundant amount of literature of empirical correlations exists for both quantities (see, for example, [27, 28, 29, 11]), one will hardly find a case for which the used boundary conditions or geometries exactly match those of the literature correlations. Due to this reason, a multi-parameter optimization routine is applied which finds the values resulting in the lowest deviation between modelled and measured reflection coefficient for all parameter combinations investigated. A genetic algorithm minimizes the function

$$\Delta = R_{\mathrm{measured}}(\boldsymbol{\omega}, \boldsymbol{A}, \boldsymbol{P}) - R_{\mathrm{model}}(\boldsymbol{\omega}, \boldsymbol{A}, \boldsymbol{P}, \boldsymbol{L_v}, \boldsymbol{\zeta}), \tag{4}$$

over the ranges of acoustic frequency $\boldsymbol{\omega}$ and excitation amplitude $\boldsymbol{A}$ of interest. This is done for several different damper geometries characterized by the geometrical parameters P_i. Finally, the optimization algorithm yields values for the end corrections $L_{v,i}$ and pressure loss coefficients ζ_i. The validity of the identified parameter values is checked by comparing model predictions to experimental results that are not used to train the model. In the model, only the physical dimensions, the bias flow velocity, and the excitation amplitude are adjusted as they are in the experiments, whereas the identified parameters for length correction and pressure loss coefficients remain constant. Note, this does not mean that the absolute value for the length correction is constant for all configurations but the identified dependency of the length correction as a function of, e.g., neck diameter remains the same.

Depending on the pulsation amplitude inside the rig or engine the damper's response might become non-linear. If the acoustic velocity inside the necks is of the order or larger than the main flow velocity, non-linear effects have to be considered. This is accounted for in the model. Figure 4 shows the reflection coefficient for different excitation amplitudes. The excitation amplitude A_0 represents the linear case – the amplitude ratio of fluctuating to static pressure inside the rig is approximately 0.025%. Although relatively small for the configuration considered here, the model (solid) nicely captures the non-linear effect caused by a 14-times higher excitation amplitude that is observed in the experiments (dashed with symbols).

The model is also capable to reproduce the effects of varying bias flow velocity. In Fig. 5, results for a variation of $\pm 50\%$ are shown. Both the resonance frequency and the magnitude of the reflection coefficient are considerably altered. The model excellently agrees with the experimental observations. Note that in contrast to single-volume dampers, for multi-volume configurations, a change of bias flow velocity also influences the resonance frequency. For the former, it only changes the magnitude of the reflection coefficient.

Above reported results proof that the physics-based model is able to describe the damping

This is a pre-print version. Published in *Journal of Engineering for Gas Turbine and Power* (2014) Vol. 136 (4) Article number 041504, DOI: 10.1115/1.4025761

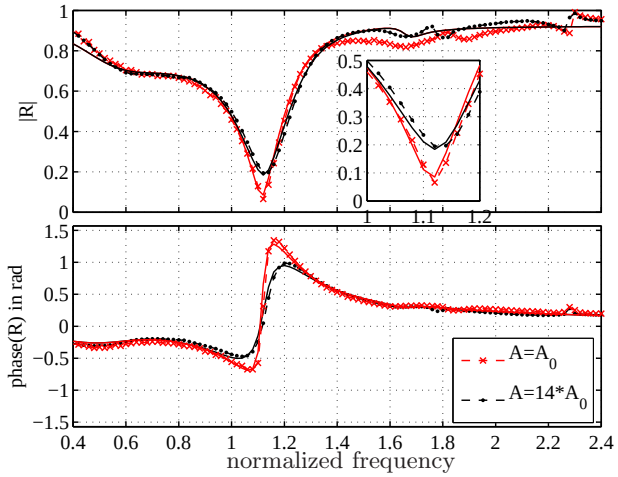

Figure 4: Comparison of measured reflection coefficients (dashed with symbols) and model (solid) for different excitation amplitudes; top: magnitude, bottom: phase.

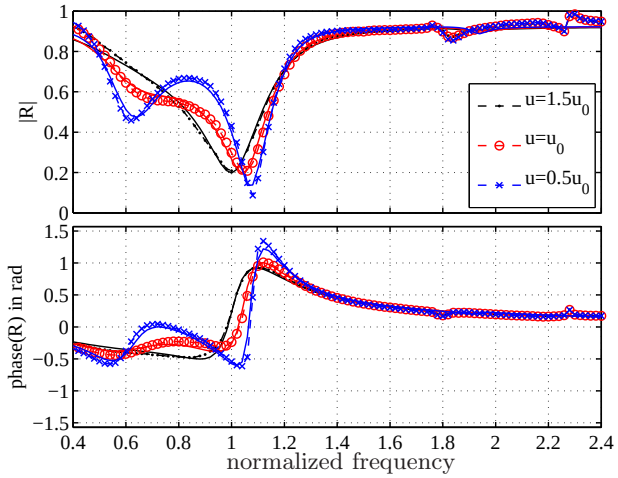

Figure 5: Comparison of measured reflection coefficients (dashed with symbols) and model (solid) for different bias flow velocities; top: magnitude, bottom: phase.

This is a pre-print version. Published in *Journal of Engineering for Gas Turbine and Power* (2014) Vol. 136 (4) Article number 041504, DOI: 10.1115/1.4025761

characteristic of all measured parameter variations. These are chosen to cover the whole range of relevant parameter combinations. Hence, this enables to perform a subsequent optimization to find the optimum geometrical dimensions and bias flow to achieve a certain damping objective. For this purpose, the coupled system damper/engine is modelled similar to approach described in Ref. [19] (see also next chapter for more details).

The damping performance is assessed by means of the growth rate reduction the dampers induce in one (or more) frequency band(s). The genetic optimization routine finds the parameter configuration (both for geometry and bias flow) yielding the maximum growth rate reduction. This is exemplarily depicted in Fig. 6. It shows the isosurfaces of the growth rate reduction integrated over the specified weighting of frequency regions. For visualization, it is shown as a function of the

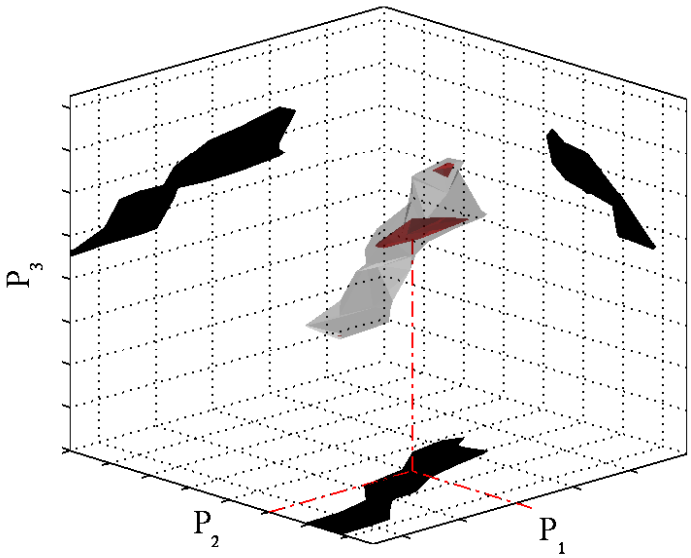

Figure 6: Isosurfaces of damping performance versus combination of geometry parameters P_1, P_2, and P_3. Red (grey) isosurface: 95% (90%) of maximum growth rate reduction.

geometrical parameters P_1, P_2, and P_3 only. In reality, the optimization was conducted for more parameters. The parameters P_i represent three dimensions (e.g., diameter, length of a secondary neck and volume ratio). In order to further visualize the three-dimensional volume enclosed by the isosurface, the projections onto each of the cartesian planes are depicted in black. All parameter combinations enclosed by the red surfaces represent possible configurations yielding 95% of the maximum achievable growth rate reduction. Accordingly, those on the grey isosurface give the parameter combination for which the damping capacity is 90% of the maximum. By doing so, the sensitivity on each of the parameters can be assessed. In addition, in case several "islands" of

This is a pre-print version. Published in *Journal of Engineering for Gas Turbine and Power* (2014) Vol. 136 (4) Article number 041504, DOI: 10.1115/1.4025761

maximum performance exist, the one providing the largest margin is taken. The red lines mark the final parameter configuration chosen for the engine tests.

Model accuracy in full-scale engine

To further validate the model of the damper placed in the engine, damper and combustion chamber are equipped with pulsation sensors (see Fig. 1). The ratio of the measured acoustic pressure inside the HHD and the one in the combustion chamber can be seen in Fig. 7 (black). It is compared to the predictions of the state-space model (red) which has an order of 6. Model

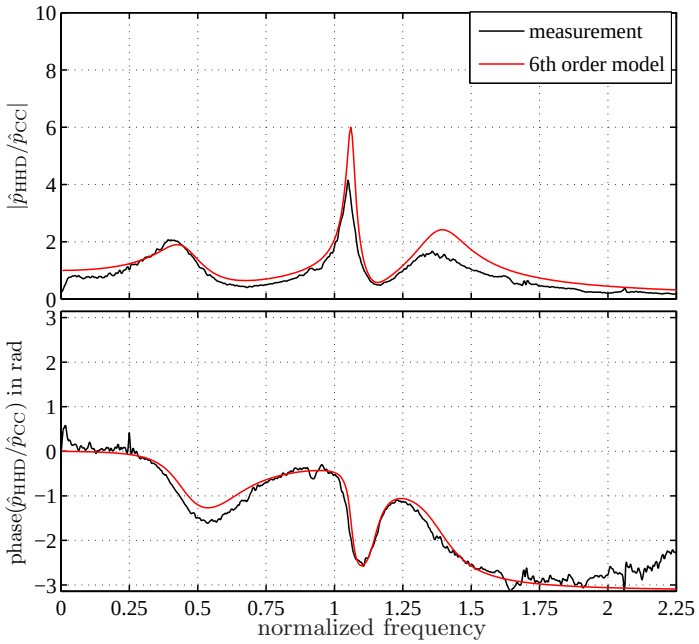

Figure 7: Comparison of ratios of acoustic pressures inside HHD and combustion chamber for measurement (black) and 6th order model (red). Top: Magnitude, bottom: phase.

predictions and measurements show a striking correspondence, thus, proving the validity and accuracy of the method proposed to obtain the damper's performance in the engine. Particularly, the phases (bottom) nearly perfectly match which is most important for the prediction of the dampers resonance frequency when mounted in the engine. Except for the deviation at a normalized frequency of 1.05, the magnitudes match very well up to 1.25. The main reason for the larger deviation at higher frequencies is the axial distance between both sensors. This is not accounted for in the model as it relates the pressure inside the HHD to that directly at its exit. For frequencies larger 1.25, this distance corresponds nearly to a quarter wave length. Note that no model tuning is

This is a pre-print version. Published in *Journal of Engineering for Gas Turbine and Power* (2014) Vol. 136 (4) Article number 041504, DOI: 10.1115/1.4025761

done a posteriori; the model prediction in Fig. 7 is obtained with the model validated for cold-flow measurements and taken for the damper layout.

4. Single- versus Multi-volume damper

Figure 8 compares the damping performances of single-volume and multi-volume dampers. The only difference between the two configurations is that the volume for the former is not subdivided into several interconnected volumes. Both setups exhibit the same total volume and geometry of the neck between damper and combustion chamber. For a meaningful assessment, this is important since the volume ratio of damper to combustion chamber is a crucial parameter for the damping performance. The neck geometry influences the broadness of the damper's frequency bandwidth. The engine is modelled as a second order harmonic oscillator; an assumption which is valid if only

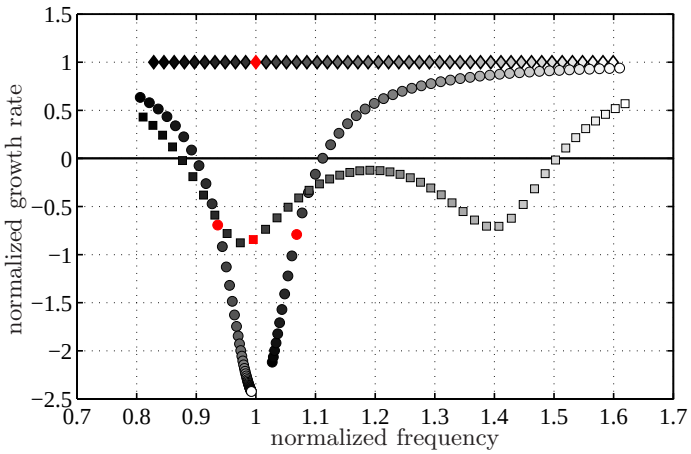

Figure 8: Normalized growth rate versus normalized frequency for system without dampers (◊), equipped with single-volume (○), and multi-volume (□) dampers.

the fundamental mode is considered. The acoustic transfer function of the damper is coupled to the engine and the least stable mode's poles of the closed-loop system – representing growth rate and oscillation frequency – are deduced. For the simulation, it is assumed that 12 dampers are evenly distributed around the combustion chamber circumference.

In Fig. 8, the growth rate of the system without dampers is normalized to unity. The model is used to vary the normalized pulsation frequency of the engine continuously from approx. 0.85 (black symbols) to 1.6 (white symbols) in order to study the damper performance at off-design frequencies or in case more than one mode has to be addressed. In reality, a change in pulsation frequency can, for instance, be caused by engine-to-engine variations, different operating or ambient conditions. As can be seen from the corresponding reflection coefficients plotted in Fig. 9, the normalized

This is a pre-print version. Published in *Journal of Engineering for Gas Turbine and Power* (2014) Vol. 136 (4) Article number 041504, DOI: 10.1115/1.4025761

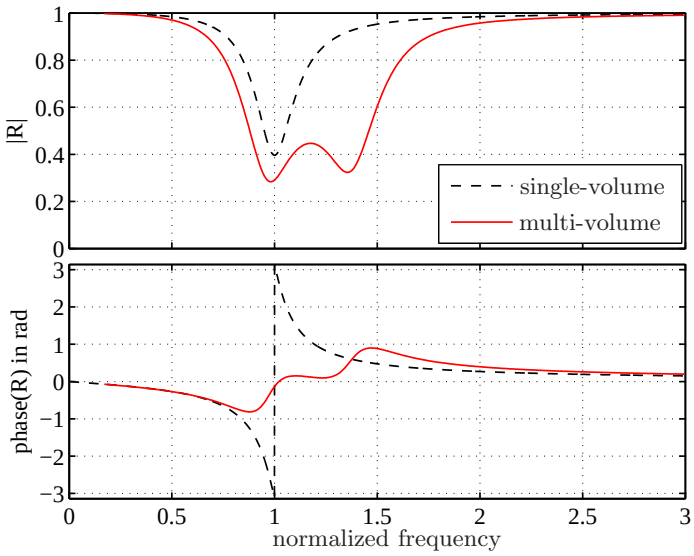

Figure 9: Comparison of reflection coefficients for single-volume (black dashed) and multi-volume (red solid) damper; top: magnitude, bottom: phase.

resonance frequency of the single-volume damper is at 1 (black dashed). The red curve represents the reflection coefficient for the multi-volume damper.

Figure 8 compares the results for the growth rate reduction obtained with the single-volume damper configuration with those of the multi-volume setup. Application of the former results in a split of the poles; the typical result one would expect for two coupled second order harmonic oscillators (refer, for instance, to citeBanaszuk2006,Rowley2006a. In case the single-volume damper's resonance frequency is exactly matching the engine pulsation frequency (red symbols), the poles are symmetrically shifted to 0.93 and 1.07. Both have a negative growth rate, thus, the system is stable. In the example shown, the growth rate reduction is a bit higher than for the multi-volume configuration. If the engine's pulsation frequency is shifted by $\pm 6\%$, the single-volume dampers are still able to maintain system stability. For larger frequency shifts, however, one of the poles gets unstable.

For the multi-volume dampers, two main observations can be made. First, no pole-splitting occurs. The reason for this can be understand by considering the phase of the reflection coefficient in the bottom graph of Fig. 9. Nearly over the whole range of frequencies for which $|R| < 0.5$, it is close to zero. In terms of acoustic impedance[1] this corresponds to the case for which its imaginary part, its reactance, is zero. A purely real-valued impedance, i.e., one that only has a resistive part, merely absorbs the acoustic energy. In contrast to this, the phase of the single-volume damper

[1]The acoustic impedance Z is related to the reflection coefficient R by the bilinear transform $Z/\rho c = (1+R)/(1-R)$.

This is a pre-print version. Published in *Journal of Engineering for Gas Turbine and Power* (2014) Vol. 136 (4) Article number 041504, DOI: 10.1115/1.4025761

exhibits a phase jump and at resonance is π. The slope of the phase is determined by the provided damping which is a function of $\zeta\bar{u}$.

Rowley & Williams [31] argue that in any feedback controlled linear system the reduction of system amplitudes (growth rates) is accompanied by an increase of growth rates at other frequencies. For a narrowband controller tuned to damp the uncontrolled system's frequency this results in the occurrence of split poles close to the undamped oscillations. Bellucci [11] derived a simple analytical formula to calculate the split poles' frequencies. His result is valid for lightly damped resonators but could also be extended to the more general case. Due to the real-valued impedance of the multi-volume damper and its broad damping characteristic the system's growth rate is decreased without a marked shift in frequency. Secondly, the frequency bandwidth in which the system is rendered stable is much larger. A shift of the non-dimensional frequency of approx. -15% to 50% can be coped with. Apart from the growth rates at a normalized frequency of 1, where both configuration result in comparable growth rates, the reduction with the multi-volume dampers is larger, hence, a system with a higher growth rate can be stabilized.

Clearly, the broadband behaviour of the single-volume configuration could be enhanced by not adjusting all single dampers to the same frequency (obviously with a pay-off in damping at this frequency). However, this would involve several different damper designs – a fact that is clearly not desired for reasons of complexity. In addition, the relevant pulsation modes important in this work are of annular nature. Depending on the critical mode shape and the number of dampers that the engine can be equipped with, a minimum number of dampers addressing the same mode or frequencies not too far away from each other is required.

5. Damper validation in engine

The performance of the multi-volume dampers is validated in a test engine. In the top frame of Fig. 10, the normalized frequency of the limiting mode as a function of two engine operating parameters $\mathcal{A}$ and $\mathcal{B}$ is shown. As can be seen the frequency increases with decreasing $\mathcal{A}$ and increasing $\mathcal{B}$ ($\mathcal{B}_1 < \mathcal{B}_2 < \mathcal{B}_3$).

In order to decrease emissions, operating parameter $\mathcal{A}$ should be minimized. The dashed curves are isolines of parameter $\mathcal{B}$ at which dedicated measurement points are taken ($\times$). The area shaded in gray in the top frame marks the operating window without dampers. Although not shown here, below the lowest $\mathcal{B}$ curve operation is always possible. The larger $\mathcal{B}$, the larger is the minimum achievable $\mathcal{A}$. Thus, the major damping objective is to sufficiently increase the operating window along $\mathcal{B}_3$.

Implementing the dampers allows to widely increase the operating window of the engine to also cover the red shaded area (Fig. 10 mid frame). Measurement points with dampers are depicted with $\circ$. Since in the red shaded area no measurement points without dampers can be taken, the frequency for the respective combination of $\mathcal{A}$ & $\mathcal{B}$ for the case without dampers is expected to be on the extrapolations of the $\mathcal{B}$-isolines. As can be seen the frequency of the former limiting

This is a pre-print version. Published in *Journal of Engineering for Gas Turbine and Power* (2014) Vol. 136 (4) Article number 041504, DOI: 10.1115/1.4025761

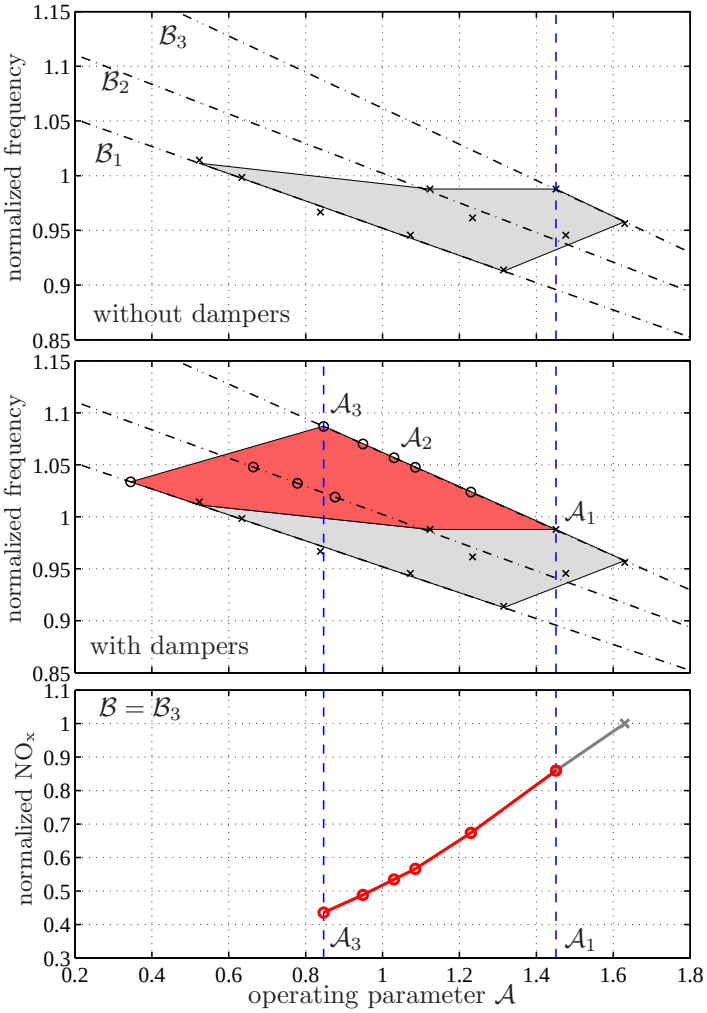

Figure 10: Normalized frequency of critical mode without dampers and NO_x versus operating parameters $\mathcal{A}$ and $\mathcal{B}$. Top: Operating window of engine without dampers. Middle: Enlarged operating window by using dampers. Bottom: Normalized NO_x improvement at $\mathcal{B}_3$ using dampers.

This is a pre-print version. Published in *Journal of Engineering for Gas Turbine and Power* (2014) Vol. 136 (4) Article number 041504, DOI: 10.1115/1.4025761

mode changes by ±10% if the averaged frequency is normalized to 1. In the whole operating range shown, the dampers are able to reduce the pulsations by at least 50% to more than 80%.

The bottom subfigure of Fig. 10 shows the reduction of normalized NO_x emissions at $\mathcal{B}_3$. Implementation of the multi-volume dampers results in a reduction of more than 55%.

Note that for the shown graph the ambient conditions are constant. Tests at different ambient conditions involve additional changes in frequency. The dampers excellently perform at these lower frequencies, too.

The engine can be equipped with a given number of N dampers. Their effect on the pulsation spectrum at operating condition $\mathcal{A}_1$ (see Fig. 10) is depicted in Fig. 11(a). Without dampers

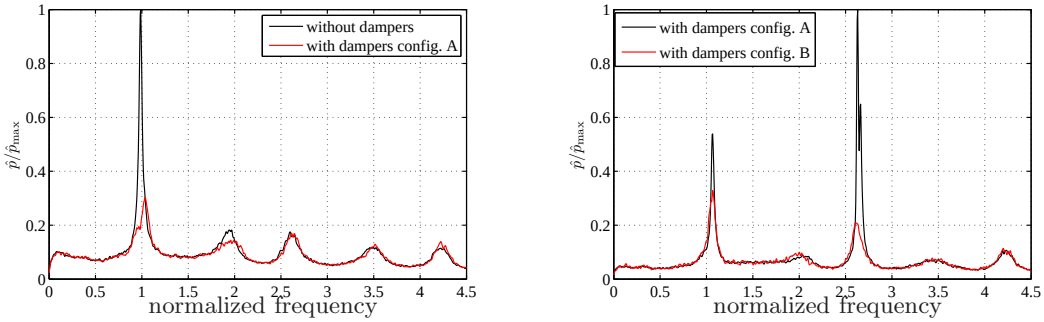

(a) Operating parameter $\mathcal{A} = \mathcal{A}_1$

(b) Operating parameter $\mathcal{A} = \mathcal{A}_2 < \mathcal{A}_1$

Figure 11: Averaged spectra of scaled acoustic pressure $\hat{p}/\hat{p}_{\max}$ for two different operating conditions.

(black), a distinct peak is observed at the frequency of the 1^{st} azimuthal mode. With 75% of the available dampers, this peak is attenuated by approximately 70% (red) allowing to reduce the operating parameter $\mathcal{A}$ by 30% to $\mathcal{A}_2$ (Fig. 10). The remaining ones are tuned to the 2^{nd} azimuthal mode; the effect being observable at a normalized frequency of approximately 2.

Obviously, further decreasing operating parameter $\mathcal{A}$ gives rise to the 1^{st} azimuthal mode. However, this mode is not the limiting anymore. Now, the amplitude of the 3^{rd} azimuthal mode becomes dominant as can be seen in Figure 11(b) (black). The reason for this is most probably twofold. First, it indicates that the system has more than one unstable eigenvalue. If a system exhibits more than one linearly unstable pole, its limit-cycling state is governed by the dominating one. This often is – but not necessarily has to be – the one with the highest growth rate. Without dampers, the 1^{st} azimuthal mode determines the limit-cycle oscillations (most probably because it has the higher growth rate). Furthermore, the dampers strongly decrease its growth rate so that the 3^{rd} azimuthal mode becomes the one governing the limit-cycle oscillations. A comparable behaviour was already observed in $Ta3$ simulations reported earlier in [23]. The stabilization of the initially unstable mode caused a second one to become dominant.

Depending on the shape of the mode causing high-amplitude pulsations the positions of the

This is a pre-print version. Published in *Journal of Engineering for Gas Turbine and Power* (2014) Vol. 136 (4) Article number 041504, DOI: 10.1115/1.4025761

dampers have to be determined. In gas turbines, often azimuthal modes are the critical ones. These modes exhibit pressure nodes around the circumference. If dampers are arranged such that the nodal points of the mode coincide with the damper positions, no damping is achieved. In a previous publication [21], azimuthal staging concepts of dampers and fuel injection in annular systems were studied in detail. It was shown that the degree of symmetry of an azimuthal distribution of damping devices allows to predict its damping capability. This degree of symmetry is defined by the parameter C_{2n}. The smaller this value for the considered thermoacoustic mode is, the higher is the damping performance. Consequently, for the respective application, the dampers have to be positioned such that the corresponding C_{2n} value is minimal. Note that in practice there will be multiple constraints probably impeding to go for the best calculational configuration. Possible constraints are, for instance, the restriction to put dampers on certain locations or insufficient space resulting in a limited number of dampers.

Given the engine pulsation behaviour at operating condition $\mathcal{A}_2$ (Fig. 11(b) black), consequently, the dampers initially adjusted to the 2^{nd} azimuthal mode are re-adjusted to deal with the 3^{rd}. Prior to engine tests, the optimum configuration resulting in the lowest C_{2n} values for both modes simultaneously is assessed. Figure 12 shows the C_{2n} values for six possible damper distributions. In the graph, it is normalized with its theoretical maximum $C_{2n,\max}$ representing

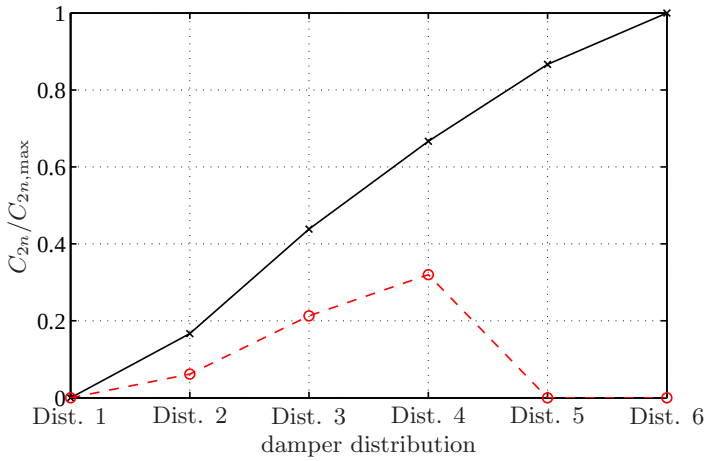

Figure 12: C_{2n} values for distributions 1-6 of damper configuration B. Black solid with $\times$: 3^{rd} azimuthal mode, red dashed with $\circ$: 1^{st} azimuthal mode. The values are scaled with the maximum C_{2n} for the respective mode.

the worst case distribution for the respective mode and number of dampers considered. For the 1^{st} azimuthal mode (red dashed with $\circ$), there are three different positions (distributions $1, 5, 6$) resulting in the optimum damping performance. Distribution 6 is chosen to address the 1^{st} azimuthal mode in damper configuration A. The reason for this is that for this distribution also the 2^{nd} azimuthal mode is damped best.

This is a pre-print version. Published in *Journal of Engineering for Gas Turbine and Power* (2014) Vol. 136 (4) Article number 041504, DOI: 10.1115/1.4025761

However, if also the 3^{rd} azimuthal mode (black solid with $\times$) has to be accounted for, distribution 6 is not optimal anymore. For this damper arrangement, the dampers addressing the 3^{rd} azimuthal mode exhibit an even spacing of 60 degrees between each other. As expected, this is the worst case distribution because the circumferential distance of the mode's nodes coincide with that of the damper locations. Merely considering the 1^{st} azimuthal mode, distribution 5 and 6 would also deliver optimum damping. However, as can be seen in the graph, the scaled C_{2n} values for the 3^{rd} azimuthal mode are worst – $C_{2n}/C_{2n,\max} = 1$. Decreasing the degree of symmetry with respect to this mode, results in a decreasing C_{2n}. The best configuration is achieved for distribution 1 for which $C_{2n}/C_{2n,\max}$ is zero for both modes.

The results shown in Fig. 11(b) (red) are obtained with the dampers arranged according to distribution 1. The pulsation amplitude of the 3^{rd} azimuthal mode is reduced by more than 80%. Since this operating condition can only be reached with dampers addressing the 1^{st} azimuthal mode, no exact quantification of its amplitude reduction compared to the case without dampers can be given. It is definitely far more than the 70% that are already observed for $\mathcal{A}_1$ (Fig. 11(a)). Note that the reason for the reduction observed at the 1^{st} azimuthal mode is due to tuning the damper to slightly higher frequencies.

6. Summary and conclusions

In this paper, a novel concept for broadband damping of low-frequency combustion pulsations in gas turbines is presented. The novel device consists of a damper body housing several volumes that are connected to each other via secondary necks. This setup results in a multi-degree-of-freedom system, for which neck geometries, bias flow, and volume ratios are subject to optimization so as to fulfill the damping objective. A physics-based model is setup which is is able to predict the influence of all governing parameters on the damping performance. The model excellently matches to cold-flow as well as full-scale engine measurements. A comparison to the performance of traditional single-volume dampers is conducted showing the benefit of the new approach.

The damper's performance is validated in a full-scale test engine. Recent research on azimuthal staging concepts [21] to address azimuthal modes is used to optimally position the dampers. Combustion pulsation amplitudes are reduced by more than 80%. By doing so, the engine operating regime is widely enlarged, finally, allowing a reduction of NO_x emissions by 55%. The engine results confirm that the dampers efficiently work in a broad frequency range. Since the novel damper concept is engine independent multiple applications are possible.

References

[1] Bellucci, V., Flohr, P., Paschereit, C. O., and Magni, F., 2004. "On the use of Helmholtz resonators for damping acoustic pulsations in industrial gas turbines". J Eng for Gas Turb Power, **126**(2), pp. 271–275.

This is a pre-print version. Published in *Journal of Engineering for Gas Turbine and Power* (2014) Vol. 136 (4) Article number 041504, DOI: 10.1115/1.4025761

[2] Bellucci, V., Schuermans, B., Nowak, D., Flohr, P., and Paschereit, C. O., 2005. "Thermoacoustic Modeling of a Gas Turbine Combustor Equipped With Acoustic Dampers". J Turbomach, **127**(2), pp. 372–379.
[3] Tam, C. K. W., Kurbatskii, K. A., Ahuja, K. K., and Jr., R. J. G., 2001. "A numerical and experimental investiagtion of the dissipation mechanisms of resonant acoustic liners". J Sound Vib, **245**(3), pp. 545–557.
[4] Eldredge, J. D., and Dowling, A. P., 2003. "The absorption of axial acoustic waves by a perforated liner with bias flow". J Fluid Mech, **485**, pp. 307–335.
[5] Randeberg, R., 2000. "Perforated panel absorbers with viscous energy dissipation enhanced by orifice design". PhD thesis, Department of Telecommunications, Norwegian University of Science and Technology. http://ntnu.diva-portal.org/smash/get/diva2:125365/FULLTEXT01.
[6] Zhang, Q., and Bodony, D. J., 2011. "Direct numerical simulation of three dimensional honeycomb liner with circular apertures". AIAA Paper 2011-843.
[7] Alster, M., 1972. "Improved calculation of resonant frequencies of helmholtz resonators". J Sound Vib, **24**(1), pp. 63–85.
[8] Huang, Y., and Yang, V., 2009. "Dynamics and stability of lean-premixed swirl-stabilized combustion". Prog Energ Combust, **35**(4), pp. 293–364.
[9] Bothien, M., Pennell, D., Zajadatz, M., and Döbbeling, K., 2013. "On key features of the AEV engine implementation for operational flexibility". ASME Paper GT2013-95693.
[10] Richards, G. A., Straub, D. L., and Robey, E. H., 2003. "Passive control of combustion dynamics in stationary gas turbines". J Propul Power, **19**(5), pp. 795–810.
[11] Bellucci, V., 2009. "Modeling and control of gas turbine thermoacoustic pulsations". PhD thesis, Institut für Strömungsmechanik und Technische Akustik, Technische Universität Berlin. http://opus.kobv.de/tuberlin/volltexte/2009/2414/.
[12] Gysling, D. L., Copeland, G. S., McCormick, D. C., and Proscia, W. M., 2000. "Combustion system damping augmentation with Helmholtz resonators". J Eng for Gas Turb Power, **122**(2), pp. 269–274.
[13] Lepers, J., Krebs, W., Prade, B., Flohr, P., Pollarolo, G., and Ferrante, A., 2005. "Investigation of thermoacoustic stability limits of an annular gas turbine combustor test-rig with and without Helmholtz resonators". ASME Paper GT2005-68246.
[14] Pandalai, R. P., and Mongia, H. C., 1998. "Combustion instability characteristics of industrial engine dry low emission combustion systems". AIAA Paper 1998-3379.
[15] Griffin, S., Lane, S. A., and Huybrechts, S., 2001. "Coupled helmholtz resonators for acoustic attenuation". J Vib Acoust, **123**, pp. 11–17.
[16] Xu, M. B., Selamet, A., and Kim, H., 2010. "Dual Helmholtz resonator". Appl Acoust, **71**, pp. 822–829.
[17] Jones, M. G., and L.Parrott, T., 2006. "Assessment of bulk absorber properties for multi-layer perforates in porous honeycomb liners". AIAA paper 2006-2403.
[18] Bielak, G. W., Premo, J. W., and Hersh, A. S., 1999. "Advanced turbofan duct liner concepts". NASA/CR-1999-209002.
[19] Noiray, N., and Schuermans, B., 2009. "Theoretical and experimental investigations on dampers performances for suppression of thermoacoustic oscillations". In Proc. of the 16th International Congress on Sound and Vibration.
[20] Noiray, N., Bothien, M., and Schuermans, B., 2011. "Investigation of nonlinear mechanisms driving combustion instabilities using an electro-acoustic van der pol oscillator". 7th European Nonlinear Oscillations Conference.
[21] Noiray, N., Bothien, M. R., and Schuermans, B., 2011. "Investigation of azimuthal staging

This is a pre-print version. Published in *Journal of Engineering for Gas Turbine and Power* (2014) Vol. 136 (4) Article number 041504, DOI: 10.1115/1.4025761

concepts in annular gas turbines". Combust Theor and Model, **15**(5), pp. 585–606.
[22] Noiray, N., Bothien, M., and Schuermans, B., 2010. "Analytical and numerical analysis of staging concepts in annular gas turbines". n3l – Int'l Summer School and Workshop on Non-Normal and Nonlinear Effects in Aero- and Thermoacoustics.
[23] Schuermans, B., Bellucci, V., and Paschereit, C. O., 2003. "Thermoacoustic modeling and control of multi burner combustion systems". ASME Paper 2003-GT-38688.
[24] Bothien, M. R., 2008. "Impedance tuning: A method for active control of the acoustic boundary conditions of combustion test rigs". PhD thesis, Institut für Strömungsmechanik und Technische Akustik, Technische Universität Berlin. http://opus.kobv.de/tuberlin/volltexte/2009/2105/.
[25] Antoulas, A., and Sorensen, D., 2001. "Approximation of large-scale dynamical systems: An overview". Int J Appl Math Comp, **11**(5), pp. 1093–1121.
[26] Paschereit, C. O., Schuermans, B., Polifke, W., and Mattson, O., 2002. "Measurement of transfer matrices and source terms of premixed flames". J Eng for Gas Turb Power, **124**(2), pp. 239–247.
[27] Idelchik, I. E., 1986. Handbook of Hydraulic Resistance, 2nd ed. Hemisphere Publishing Corporation.
[28] Peters, M. C. A. M., Hirschberg, A., Reijnen, A. J., and Wijnands, A. P. J., 1993. "Damping and reflection coefficient measurements for an open pipe at low Mach and low Helmholtz numbers". J Fluid Mech, **256**, pp. 499–534.
[29] Chanaud, R. C., 1994. "Effects of geometry on the resonance frequency of Helmholtz resonators". J Sound Vib, **178**(3), pp. 337–348.
[30] Banaszuk, A., Mehta, P., Jacobson, C., and Khibnik, A., 2006. "Limits of achievable performance of controlled combustion processes". IEEE T Contr Syst T, **14**(5), pp. 881–895.
[31] Rowley, C. W., and Williams, D. R., 2006. "Dynamics and control of high-Reynolds-number flow over open cavities". Annu Rev Fluid Mech, **38**, pp. 251–276.

This is a pre-print version. Published in *Journal of Engineering for Gas Turbine and Power* (2014) Vol. 136 (4) Article number 041504, DOI: 10.1115/1.4025761